

DreamMotion: Space-Time Self-Similarity Score Distillation for Zero-Shot Video Editing

Hyeonho Jeong¹, Jinho Chang¹, Geon Yeong Park², and Jong Chul Ye^{1,2}

¹ Graduate School of AI ² Bio and Brain Engineering
Korea Advanced Institute of Science and Technology (KAIST)
{hyeonho.jeong, jinhojsk515, pky3436, jong.ye}@kaist.ac.kr



Fig. 1: Zero-shot video editing results. The second row presents videos produced with our method with a non-cascaded video diffusion model, while those in the bottom row are from a cascaded model. For a full display of results, visit our *project page*.

Abstract. Text-driven diffusion-based video editing presents a unique challenge not encountered in image editing literature: establishing real-world motion. Unlike existing video editing approaches, here we focus on score distillation sampling to circumvent the standard reverse diffusion process and initiate optimization from videos that already exhibit natural motion. Our analysis reveals that while video score distillation can effectively introduce new content indicated by target text, it can also cause significant structure and motion deviation. To counteract this, we propose to match space-time self-similarities of the original video and the edited video during the score distillation. Thanks to the use of score distillation, our approach is model-agnostic, which can be applied for both cascaded and non-cascaded video diffusion frameworks. Through extensive comparisons with leading methods, our approach demonstrates its superiority in altering appearances while accurately preserving the original structure and motion. Project page: <https://hyeonho99.github.io/dreammotion/>

1 Introduction

Building upon the progress in diffusion models [14, 46, 49], the advent of large-scale text-image pairs [42] brought unprecedented breakthrough in text-driven image generative tasks. In particular, real-world image editing has undergone significant evolution, supported by foundational Text-to-Image (T2I) diffusion models [34, 39–41]. However, extending the success of diffusion-based image editing to video editing introduces a significant challenge: modelling temporally consistent, real-world motion throughout the reverse diffusion process.

Existing methods leveraging T2I diffusion models typically start by inflating attention layers to attend to multiple frames simultaneously [7, 8, 21, 22, 37, 56, 60, 61, 65]. Yet, this technique falls short in achieving smooth and complete motion, as it depends on the implicit preservation of motion through the inflated attention layers. As a result, commonly adopted solution is to employ additional visual hints that explicitly guide the reverse diffusion process. One strategy is to use attention map guidance, for example, by injecting self-attention maps [4, 37] or manipulating cross-attentions [28]. Other works attempt to integrate the denoising process with spatially-aligned structural cues, like depth or edge maps. For example, pretrained adapter networks such as ControlNet [64] or GLIGEN [26] have been transferred from image to video domain, achieving structure-consistent outputs [7, 17, 21, 65].

Even with the presence of pretrained Text-to-Video (T2V) diffusion models, zero-shot video editing still poses a significant hurdle since publicly available T2V models [50, 55] lack a sufficiently rich temporal prior to accurately depict real-world motion in the generated videos, as illustrated in Fig. 2. Thus, recent endeavors often adopt a self-supervised strategy of finetuning pretrained model weights on the motion presented in an input video [20, 59, 66, 68]. Whether employing T2I or T2V models, the conventional reverse diffusion process—beginning with standard Gaussian noise or, at most, inverted latent representations—struggles to reprogram complex, real-world motion, unless supplemented by additional visual conditions or by overfitting the spatial-temporal prior to a particular video.

To this end, we propose to diverge from the previous video editing literature. Our approach, DreamMotion, deliberately avoids the standard denoising process (ancestral sampling), and instead leverages the Score Distillation Sampling (SDS, [36]) grounded optimization to edit a video. Specifically, starting from an input video with temporally-consistent, natural motion, we attempt to progressively modify the video’s appearance while maintaining the integrity of the motion. In specific, our framework gradually injects target appearance to the video using Delta Denoising Score (DDS, [11]) gradients within T2V diffusion models. During this procedure, we filter the gradients with additional binary mask conditions to avoid blurriness and over-saturation. While this optimization effectively infuses the targeted appearance, it tends to accumulate structural errors, resulting in deviations in motion across the final output frames (see Fig. 3). To address this, we present self-similarity-based space-time regularization methods. More specifically, by aligning the spatial self-similarity of



Fig. 2: Ancestral sampling based zero-shot video editing fails to capture complex, real-world motion in the generated videos.

diffusion features between the original and edited videos, we preserve structure and motion integrity while seamlessly modifying the appearance. Furthermore, ensuring temporal self-similarity between the two features facilitates effective temporal smoothing, preventing potential distortions in areas subjected to optimization. Our methodology is applied to both cascaded and non-cascaded video diffusion models, showcasing its wide applicability across different video editing frameworks.

In summary, our work offers the following key contributions:

- A pioneering zero-shot framework that distills video score from text-to-video diffusion prior to inject target appearance.
- A novel space-time regularization that aligns spatial self-similarity to minimize structural deviations and temporal self-similarity to prevent distortions.
- Comprehensive validation of our approach across two distinct setups: non-cascaded and cascaded video diffusion frameworks.

2 Background

Diffusion Models Diffusion models [14, 46, 49] define the generative process as the reverse of the forward noising process. For clean data represented by $\mathbf{x}_0 \sim p_{\text{data}}(\mathbf{x})$, the forward process gradually introduces Gaussian noise through Markov transition with conditional densities

$$\begin{aligned} p(\mathbf{x}_t | \mathbf{x}_{t-1}) &= \mathcal{N}(\mathbf{x}_t | \beta_t \mathbf{x}_{t-1}, (1 - \beta_t) \mathbf{I}), \\ p(\mathbf{x}_t | \mathbf{x}_0) &= \mathcal{N}(\mathbf{x}_t | \sqrt{\bar{\alpha}_t} \mathbf{x}_0, (1 - \bar{\alpha}_t) \mathbf{I}), \end{aligned} \quad (1)$$

where $\mathbf{x}_t \in \mathbb{R}^d$ is a noised latent representation at timestep t and the noise schedule β_t is a monotonically increasing sequence of t with $\alpha_t := 1 - \beta_t$, $\bar{\alpha}_t := \prod_{i=1}^t \alpha_i$. Then, the objective of diffusion model training is to obtain a multi-scale U-Net denoiser ϵ_{ϕ^*} that satisfies

$$\phi^* = \arg \min_{\phi} \mathbb{E}_{\mathbf{x}_t \sim p_t(\mathbf{x}_t | \mathbf{x}_0), \mathbf{x}_0 \sim p_{\text{data}}(\mathbf{x}_0), \epsilon \sim \mathcal{N}(0, \mathbf{I})} [\|\epsilon_{\phi}(\mathbf{x}_t, t) - \epsilon\|_2^2], \quad (2)$$

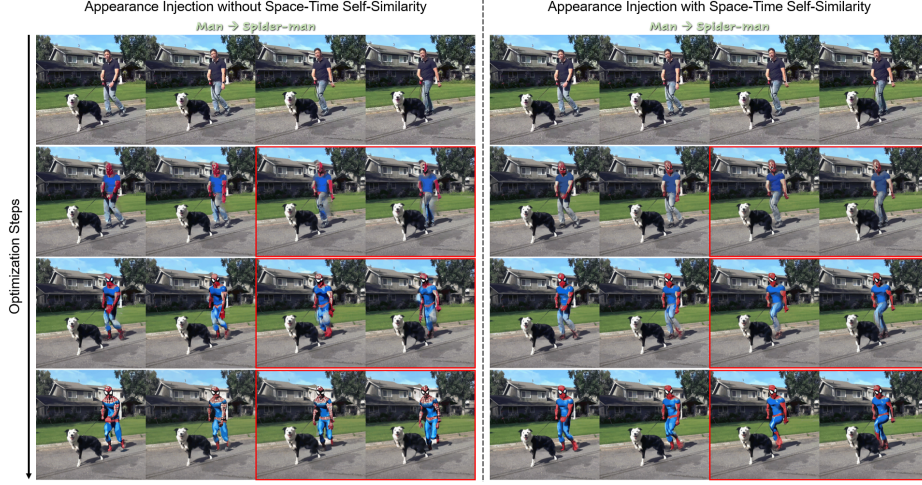


Fig. 3: Optimization progress visualization. The proposed self-similarity regularization effectively preserves the structure and motion of the original video.

where $\epsilon_{\phi^*}(\mathbf{x}_t, t) \simeq \epsilon = \frac{\mathbf{x}_t - \sqrt{\bar{\alpha}_t} \mathbf{x}_0}{\sqrt{1 - \bar{\alpha}_t}}$. Notably, the Epsilon-Matching loss in (2) is equivalent to the Denoising Score Matching (DSM, [19, 48, 54]) with alternative parameterization:

$$\min_{\phi} \mathbb{E}_{\mathbf{x}_t, \mathbf{x}_0, \epsilon} \left[\left\| \mathbf{s}_{\phi}^t(\mathbf{x}_t) - \nabla_{\mathbf{x}_t} \log p_t(\mathbf{x}_t | \mathbf{x}_0) \right\|_2^2 \right], \quad (3)$$

where $\mathbf{s}_{\phi^*}(\mathbf{x}_t, t) \simeq -\frac{\mathbf{x}_t - \sqrt{\bar{\alpha}_t} \mathbf{x}_0}{1 - \bar{\alpha}_t} = -\frac{1}{\sqrt{1 - \bar{\alpha}_t}} \epsilon_{\phi^*}(\mathbf{x}_t, t)$. For the reverse process, with the learned noise prediction network ϵ_{ϕ}^* , the noisy sample of previous timestep \mathbf{x}_{t-1} can be estimated by:

$$\mathbf{x}_{t-1} = \frac{1}{\sqrt{\alpha_t}} \left(\mathbf{x}_t - \frac{1 - \alpha_t}{\sqrt{1 - \bar{\alpha}_t}} \epsilon_{\phi^*}(\mathbf{x}_t, t) \right) + \tilde{\beta}_t \epsilon, \quad (4)$$

where $\tilde{\beta}_t := \frac{1 - \bar{\alpha}_{t-1}}{1 - \bar{\alpha}_t} \beta_t$ and $\epsilon \sim \mathcal{N}(0, \mathbf{I})$.

Conditional Generation In the context of conditional generation, data \mathbf{x} is paired with an additional conditioning signal y , which in our case is a text caption. To train a text-driven diffusion model, the text conditional embedding y is incorporated to the objective as:

$$\min_{\phi} \mathbb{E}_{\mathbf{x}_t, \mathbf{x}_0, \epsilon, y} \left[\left\| \epsilon_{\phi}(\mathbf{x}_t, t, y) - \epsilon \right\| \right] \quad (5)$$

To augment the effect of text condition, classifier-free guidance [15] attempts to benefit from both conditional and unconditional noise prediction, using a single network. In specific, the epsilon prediction is defined as

$$\epsilon_{\phi}^w(\mathbf{x}_t, t, y) = (1 + w) \epsilon_{\phi}(\mathbf{x}_t, t, y) - w \epsilon_{\phi}(\mathbf{x}_t, t, \emptyset), \quad (6)$$

where \emptyset denotes null text embedding and w is the guidance scale.

Video Diffusion Models Our framework leverages foundational video diffusion models for obtaining video score. Consider a video sequence of N frames represented by $\mathbf{x}^{1:N} \in \mathbb{R}^{N \times d}$. For any n -th frame within this sequence, denoted by $\mathbf{x}^n \in \mathbb{R}^d$, the noisy frame latent \mathbf{x}_t^n sampled from $p_t(\mathbf{x}_t^n | \mathbf{x}^n)$ can be expressed as $\mathbf{x}_t^n = \sqrt{\bar{\alpha}_t} \mathbf{x}^n + \sqrt{1 - \bar{\alpha}_t} \boldsymbol{\epsilon}_t^n$, where $\boldsymbol{\epsilon}_t^n \sim \mathcal{N}(0, I)$. Then, we similarly define $\mathbf{x}_t^{1:N}$ and $\boldsymbol{\epsilon}_t^{1:N}$. The objective of video diffusion model training is then to obtain a denoiser network ϵ_{ϕ^*} that satisfies:

$$\phi^* = \arg \min_{\phi} \mathbb{E}_{\mathbf{x}_t^{1:N}, \mathbf{x}^{1:N}, \boldsymbol{\epsilon}_t^{1:N}, y} [\|\epsilon_{\phi}(\mathbf{x}_t^{1:N}, t, y) - \boldsymbol{\epsilon}^{1:N}\|], \quad (7)$$

where y is a text caption uniformly describing the video sequence $\mathbf{x}^{1:N}$.

Seeking to create videos that are both spatially and temporally enlarged and of high quality, video diffusion models have been expanded to cascaded pipelines [2, 13, 16, 45, 57, 63]. These cascaded video pipelines commonly follow a coarse-to-fine video generation approach, beginning with a module dedicated to creating keyframes that are low in both spatial and temporal resolution. Subsequent stages involve temporal interpolation and spatial super-resolution modules, which work to increase the temporal and spatial resolution of the frames, respectively. In this work, we plug our method to both cascaded and non-cascaded scenarios, proving its model-agnostic capability.

3 DreamMotion

3.1 Overview

Starting with a series of input video frames $\hat{\mathbf{x}}^{1:N}$, a corresponding text prompt \hat{y} , and a target text y , our goal is to get an edited video $\mathbf{x}^{1:N}$ that preserves the structural integrity and overall motion of $\hat{\mathbf{x}}^{1:N}$, while faithfully reflecting y . DreamMotion starts by initializing the target video variable $\mathbf{x}_0^{1:N}(\theta)$ by the original video $\hat{\mathbf{x}}^{1:N}$. Our optimization strategy is then three-pronged: (1) \mathcal{L}_{V-DDS} that paints $\mathbf{x}_0^{1:N}(\theta)$ to match the appearance dictated by y , (2) \mathcal{L}_{S-SSM} which encourages the structure of $\mathbf{x}_0^{1:N}(\theta)$ to align with $\hat{\mathbf{x}}^{1:N}$, (3) \mathcal{L}_{T-SSM} which smoothens the gradients over temporal dimension to eliminate any potential artifacts.

In Sec. 3.2, we briefly review SDS and DDS loss formulations, and describe how we directly modify appearance of $\mathbf{x}^{1:N}$ with DDS-based gradients. This technique, while effective in appearance injection, tends to accumulate structural inaccuracies, resulting in motion deviation in the end output. To address this, Sec. 3.3 introduces a strategy for structural correction based on self-similarity, and Sec. 3.4 details our approach for temporal smoothing, also leveraging self-similarity. Finally, in Sec. 3.5, we elaborate on the extension of DreamMotion to the cascaded video diffusion framework. For simplicity, we primarily describe the diffusion model as operating in pixel space throughout this paper. However, in practice, our implementation encompasses both a latent-space based (Sec. 4.1, [50]) and a pixel-space based video diffusion model (Sec. 4.2, [63]).

3.2 Appearance Injection

Image Score Distillation Let $\mathbf{x}_0(\theta)$ denote the target image parameterized by θ and ϵ_{ϕ} represent a T2I diffusion model. SDS aims to align $\mathbf{x}_0(\theta)$ with the

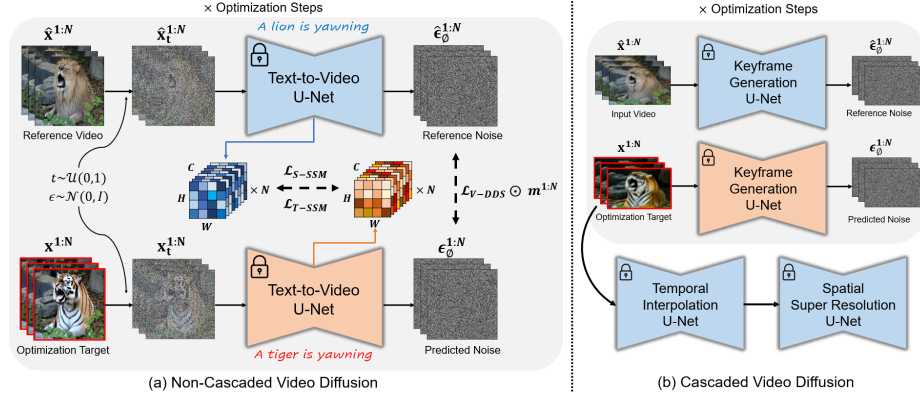


Fig. 4: Overview. DreamMotion leverages gradients derived from score distillation to inject target appearance, which is complemented by self-similarity alignments across spatial and temporal dimensions. This strategy seamlessly fits into cascaded video diffusion frameworks, confining the optimization on the keyframe generation phase.

target text y by optimizing the diffusion training loss gradient, expressed as:

$$\mathcal{L}_{\text{SDS}}(\theta; y) = \|\epsilon_\phi^w(\mathbf{x}_t(\theta), t, y) - \epsilon\|_2^2, \quad (8)$$

with $\epsilon \sim \mathcal{N}(0, \mathbf{I})$ and $t \sim \mathcal{U}(0, 1)$. Although $\nabla_\theta \mathcal{L}_{\text{SDS}}$ provides an efficient gradient term for incrementally refining the image fidelity to the text y , SDS often results in over-saturation, blurriness, and lack of details in the generated image [11, 23, 27, 32, 58].

Under the assumption that the SDS score should be zero for pairs of correctly matched prompts and images, DDS [11] enhances the gradient direction obtained from the SDS framework by incorporating an additional text-image pair, comprising a reference text \hat{y} and a reference image $\hat{\mathbf{x}}_0$. Specifically, the noisy direction of SDS score is calculated using the reference text-image branch, and this noisy score is subtracted from the main SDS optimization branch:

$$\mathcal{L}_{\text{DDS}}(\theta; y) = \|\epsilon_\phi^w(\mathbf{x}_t(\theta), t, y) - \epsilon_\phi^w(\hat{\mathbf{x}}_t, t, \hat{y})\|_2^2. \quad (9)$$

Video Score Distillation with Masked Gradients Leveraging a pretrained T2V diffusion model ϵ_ϕ , we extend the DDS mechanism to distill video scores. Let $\mathbf{x}_0^{1:N}(\theta)$ represent the target video parameterized by θ , and $\mathbf{x}_0^{1:N}$ denote the fixed, source video. We optimize the video variable $\mathbf{x}_0^{1:N}(\theta)$ to reflect target text y by minimizing:

$$\mathcal{L}_{\text{V-DDS}}(\theta; y) = \|\epsilon_\phi^w(\mathbf{x}_t^{1:N}(\theta), t, y) - \epsilon_\phi^w(\hat{\mathbf{x}}_t^{1:N}, t, \hat{y})\|_2^2. \quad (10)$$

While the video delta denoising score (V-DDS) offers a reliable gradient for gradually injecting appearance described by target text y , it still suffers from blurriness and over-saturation. We mitigate this issue by additional mask conditioning. Specifically, we filter the obtained gradients with a sequence of masks $m^{1:N}$ that annotate the objects to be edited in each frame, by $\nabla_\theta \mathcal{L}_{\text{V-DDS}} \odot m^{1:N}$.

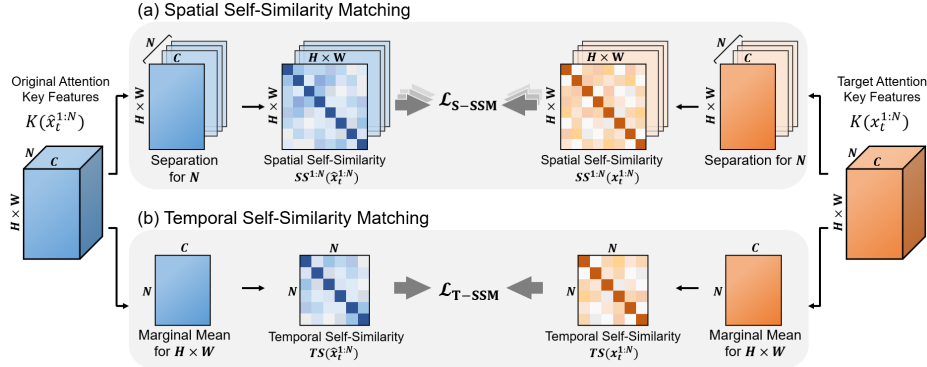


Fig. 5: The proposed space-time self-similarity regularization: (a) Spatial Self-Similarity Matching and (b) Temporal Self-Similarity Matching

The filtered gradients ensure that unintended regions in $\mathbf{x}_0^{1:N}(\theta)$ remain unaffected during V-DDS optimization (see Fig. 6).

A more significant issue arises when inaccurate gradients of \mathcal{L}_{V-DDS} accumulate structural errors throughout the optimization process. Unlike editing still images, these errors are particularly problematic in video editing, as their accumulation deters temporal consistency within frames and often results in motion deflection, as illustrated in Fig. 3, 9. To tackle this, we propose to match self-similarities between target and reference branches, as detailed in Section 3.3.

3.3 Structure Correction

Spatial Self-Similarity Matching To address structural integrity, we require a representation that remains resilient against local texture patterns while retaining the global layout and overall shape of objects: self-similarity descriptors. Self-similarity of visual features facilitates identifying objects by emphasizing the relationship of an object’s appearance to its surroundings, rather than relying on its absolute appearance. This principle of relative appearance has been effectively applied across various domains: in traditional methods for matching visual patterns [43], in the realm of neural style transfer through deep convolutional neural network features [24], and more recently, in the field of image editing utilizing DINO ViT features [3, 25, 53].

Our contribution lies in pioneering the application of self-similarity through deep diffusion features [51] to ensure structural correspondence between the target video $\mathbf{x}^{1:N}$ and the original video $\hat{\mathbf{x}}^{1:N}$. To achieve this, we add *identical noise* of timestep t to both videos (Eq. 1), resulting in $\mathbf{x}_t^{1:N}$ and $\hat{\mathbf{x}}_t^{1:N}$, which are then feed-forwarded to the video diffusion U-Net ϵ_ϕ to extract a pair of attention key features $K(\mathbf{x}_t^{1:N}), K(\hat{\mathbf{x}}_t^{1:N}) \in \mathbb{R}^{N \times (H \times W) \times C}$. Subsequently, we calculate spatial self-similarity map $SS^n(\cdot) \in \mathbb{R}^{(H \times W) \times (H \times W)}$ of each n -th frame as follows:

$$SS_{i,j}^n(\mathbf{x}_t^{1:N}) = \cos(K_i^n(x_t^{1:N}), K_j^n(x_t^{1:N})), \quad (11)$$

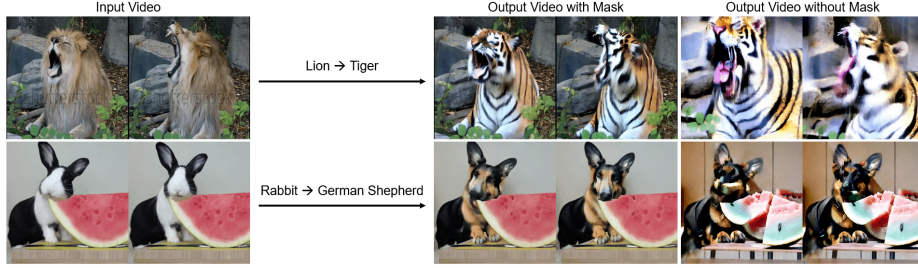


Fig. 6: Filtering optimization gradients plays a crucial role in maintaining visual fidelity and preserving structure of the input video. See Fig. 12 for full results and masks.

where $\cos(\cdot, \cdot)$ denotes the normalized cosine similarity and $\mathbf{x}_t^{1:N}(\theta)$ is simplified to $\mathbf{x}_t^{1:N}$ for brevity. The spatial self-similarity matching objective is formulated as:

$$\mathcal{L}_{\text{S-SSM}}(\mathbf{x}_t^{1:N}, \hat{\mathbf{x}}_t^{1:N}) = \frac{1}{N} \sum_{n=1}^N \left\| SS^n(\mathbf{x}_t^{1:N}) - SS^n(\hat{\mathbf{x}}_t^{1:N}) \right\|_2^2, \quad (12)$$

thereby quantifying and minimizing the discrepancy between the self-similarity maps of the target and original videos.

3.4 Temporal Smoothing

Temporal Self-Similarity Matching Although the spatial self-similarity alignment, facilitated by $\mathcal{L}_{\text{S-SSM}}$, proficiently maintains structural consistency between the original and modified videos, it operates as a frame-independent optimization method, without considering the temporal correlation between frames. As observed in Fig. 9, such per-frame operations can lead to localized distortions and notable flickering in the optimized frames. To address these artifacts, we introduce a temporal regularization of $\mathcal{L}_{\text{S-SSM}}$ that models temporal correlations by leveraging self-similarity along the frame axis.

Calculating self-similarity over time necessitates a method to compress spatial information while retaining essential spatial details. For this purpose, we employ spatial marginal mean as a first-order statistic, spatial marginal mean, as our global descriptor. This choice is supported by prior works [24, 62], which have demonstrated its effectiveness in capturing crucial spatial details and serving as a robust global descriptor. More concretely, we condense the spatial dimensions of the extracted key features $K(\mathbf{x}_t^{1:N}) \in \mathbb{R}^{N \times (H \times W) \times C}$ to $M[K(\mathbf{x}_t^{1:N})] \in \mathbb{R}^{N \times C}$ through the process defined as:

$$M[K(\mathbf{x}_t^{1:N})] = \frac{1}{H \cdot W} \sum_{i=1}^{H \cdot W} K_i(\mathbf{x}_t^{1:N}), \quad (13)$$

where H and W denote the height and width, respectively, and C represents the channel dimension of the feature maps. We then establish the temporal self-similarity $TS(\cdot) \in \mathbb{R}^{N \times N}$ as follows:

$$TS_{i,j}(\mathbf{x}_t^{1:N}) = \cos(M_i[K(\mathbf{x}_t^{1:N})], M_j[K(\mathbf{x}_t^{1:N})]). \quad (14)$$

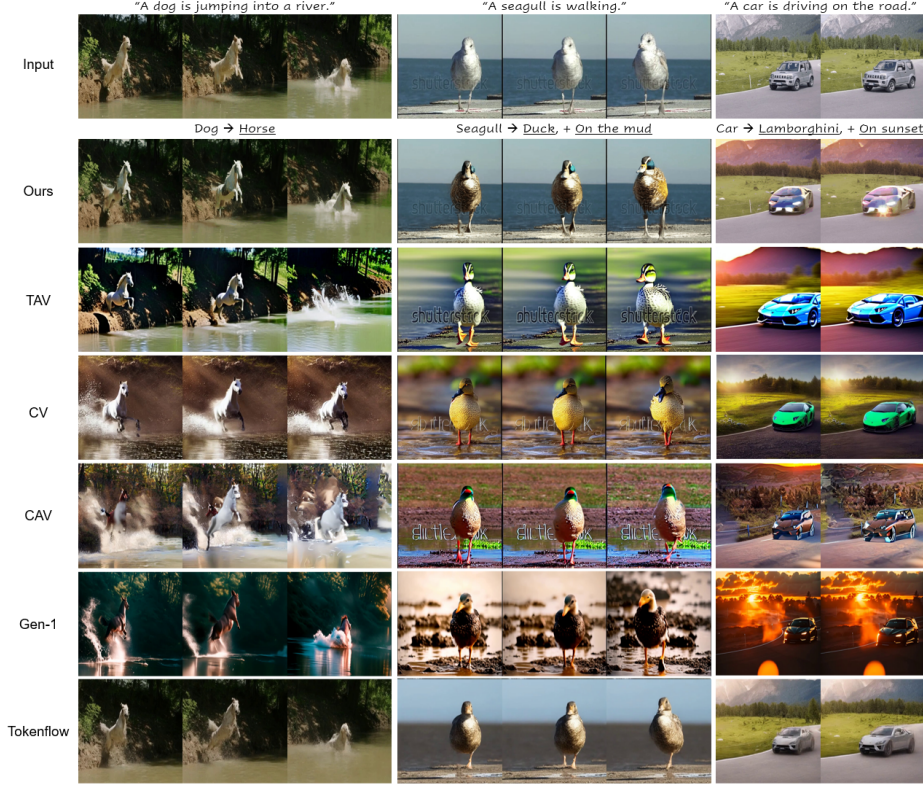


Fig. 7: Comparison. DreamMotion, applied to Zeroscope model, is evaluated against five baseline methods. For a detailed assessment, visit our project page.

Subsequently, the temporal self-similarity matching loss is formulated as:

$$\mathcal{L}_{\text{T-SSM}}(\mathbf{x}_t^{1:N}, \hat{\mathbf{x}}_t^{1:N}) = \left\| TS(\mathbf{x}_t^{1:N}) - TS(\hat{\mathbf{x}}_t^{1:N}) \right\|_2^2. \quad (15)$$

It's noteworthy that the three losses $\mathcal{L}_{\text{V-DDS}}$, $\mathcal{L}_{\text{S-SSM}}$ and $\mathcal{L}_{\text{T-SSM}}$ share the same noise ϵ and time t for their computations, achieving a computationally efficient integration of optimizations through a single forward and reverse diffusion step.

3.5 Expansion to Cascade Video Diffusion

As outlined in Section 2, cascaded video diffusion models commonly utilize a coarse-to-fine approach for video generation, comprising three specialized modules that function in sequence: Keyframe Generation, Temporal Interpolation, and Spatial Super Resolution. Rather than applying the optimization process through this comprehensive pipeline—a process that would result in prohibitively high computational costs—we focus our efforts exclusively on the initial Keyframe Generation stage. Within this approach, we reinterpret $\mathbf{x}^{1:N}$ and $\hat{\mathbf{x}}^{1:N}$ to represent, respectively, the target and original keyframes, both resized to accommo-

date the low-resolution requirements of the keyframe generation space. Furthermore, we designate ϵ_ϕ to represent the keyframe generation U-Net, excluding the temporal interpolation and super resolution modules. Following this setup, we apply our optimizations— \mathcal{LV} -DDS, \mathcal{LS} -SSM, and \mathcal{LT} -SSM—directly to $\mathbf{x}^{1:N}$. After completing the optimization, these refined keyframes undergo further processing through the Temporal Interpolation and Spatial Super Resolution stages. This comprehensive procedure is depicted in Fig. 4-(b), illustrating the streamlined approach to integrating our optimization methods within the cascaded video diffusion model framework.

4 Experiments

4.1 Non-cascaded Video Diffusion Framework

Setup For evaluation, we choose 26 text-video pairs from the public DAVIS [35] and WebVid [1] datasets. The videos vary in length from 8 frames to 16 frames. In this experiment, we deploy our method on ZeroScope [50], a foundational text-to-video latent diffusion model. The CFG scale w is configured as 9.0. We perform optimization for 200 steps using stochastic gradient descent (SGD) with learning rate of 0.4. The optimization of an 8-frame video requires approximately 2 minutes, while optimizing a 16-frame video takes around 4 minutes, utilizing a single A100 GPU.

Baselines Our method is evaluated alongside 1 one-shot and 4 zero-shot video editing baselines. Tune-A-Video (TAV, [60]) selectively finetunes attention projection layers within an inflated T2I model on the given input video. ControlVideo (CV, [65]) integrates temporally extended ControlNet [64] to T2I diffusion and achieves motion-consistent video generation without any finetuning. Both Control-A-Video (CAV, [7]) and Gen-1 [9] are video diffusion models trained on large-scale text-image and text-video data. They explicitly guide the ancestral denoising process with a series of structural conditions like depth maps. Tokenflow [10] accomplishes time-consistent video editing by enforcing uniformity on the internal diffusion features across frames, in a zero-shot manner.

Qualitative Results Fig. 7 offers a qualitative comparison between our method and state-of-the-art baselines; for complete videos, refer to our *project page*. Our method produces temporally consistent videos that closely adhere to the target prompt while most accurately preserving the motion of the input video, a feat that other baselines struggle to achieve simultaneously.

Quantitative Results We conducted a comprehensive quantitative evaluation, which includes both automatic metrics and a user study. The summarized results can be found in Tab. 1. (a) *Automatic metrics*. We employ CLIP [38] for automatic evaluation. To assess textual alignment [12], we measure the average cosine similarity between the textual prompt and the frames that have been

edited. In terms of frame consistency, we calculate CLIP image features for every frame in the output video and then compute the average cosine similarity across all pairs of frames within the video. According to the results in Tab. 1, our approach surpasses the baselines in achieving higher textual alignment and better temporal consistency. (b) *User study*. We surveyed 36 participants to assess the accuracy of editing, temporal consistency, and preservation of structure & motion, using a rating scale from 1 to 5. Participants were shown the input video followed by anonymized output videos from each baseline. They were then asked the three questions: (i) Edit Accuracy: Does the output video accurately reflect the target text by appropriately editing all relevant elements? (ii) Frame Consistency: Are the frames in the output video temporally consistent? (iii) Structure and Motion Preservation: Has the structure and motion of the input video been accurately maintained in the output video? Tab. 1 illustrates that our method outperforms the baselines in all measured aspects.

Method	Automatic Metric		Human Eval.		
	Text-Align	Frame-Con	Edit-Acc	Frame-Con	SM-Preserve
TAV	0.8177	0.9218	3.52	2.82	2.89
CV	0.7850	0.9678	2.74	2.68	2.03
CAV	0.7848	0.9297	2.17	2.16	2.18
Gen-1	0.8192	0.9704	3.31	3.62	2.95
Tokenflow	0.7813	0.9576	3.63	3.54	3.92
Ours (Zeroscope)	0.8209	0.9726	4.14	4.21	4.33
Inv + Word Swap	0.7586	0.9714	3.36	3.42	2.21
VMC	0.7563	0.9703	3.13	3.22	3.35
Ours (Show-1)	0.7747	0.9755	3.97	3.74	4.30

Table 1: Quantitative evaluations. Our method, when applied on Zeroscope, outperforms non-cascaded baselines, while our approach applied on Show-1 surpasses cascaded baselines, in all five features.

4.2 Cascaded Video Diffusion Framework

Setup In this experiment, we utilize the 8-frame videos from the previously assembled text-video pairs. Additionally, we benefit from Show-1 [63], an open-source, cascaded video diffusion model. As detailed in Sec. 3.5, we compose our cascaded pipeline comprising Keyframe Generation, Temporal Interpolation, and Spatial Super Resolution, with all modules operating in pixel-space. Our method is implemented during the initial keyframe generation stage. During keyframe optimization, these input videos undergo resizing to a resolution of 80x128 pixels, with the optimization process taking approximately 3 minutes on a single A100 GPU. Following the optimization, the frame interpolation and super-resolution modules expand the output keyframes temporally and spatially, respectively.

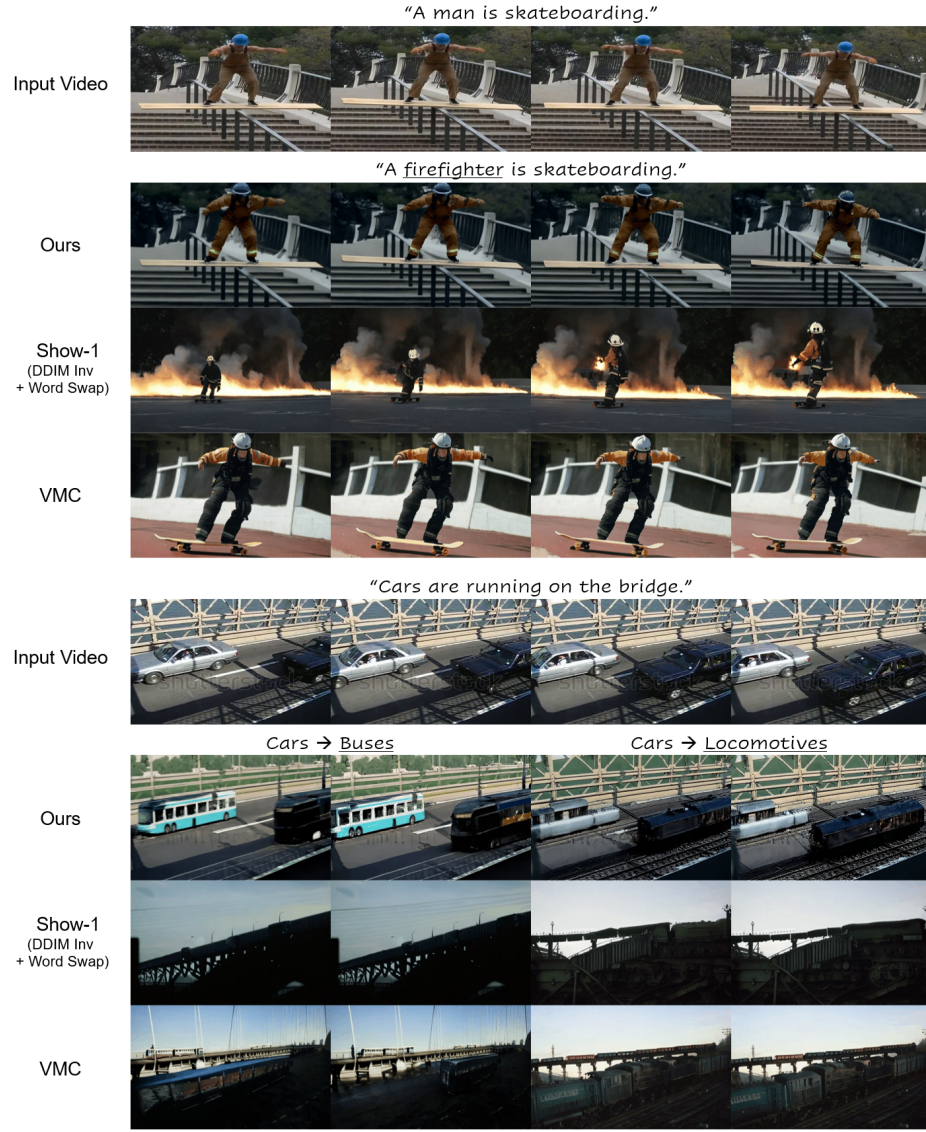


Fig. 8: Comparison. Our approach, applied to Show-1 cascaded model, is evaluated against two baselines.

Baselines To our knowledge, VMC [20] stands out as the sole video editing approach utilizing a cascaded video diffusion pipeline. VMC adapts temporal attention layers within the keyframe generation module, leveraging their novel motion distillation objective. For comparison purpose, we introduce an additional variant that employs direct inference using the cascaded pipeline with modified target text, starting from the DDIM inverted latents [47].



Fig. 9: Ablation of spatial and temporal self-similarity alignments. Joint optimization of $\mathcal{L}_{V-DDS} + \mathcal{L}_{S-SSM} + \mathcal{L}_{T-SSM}$ generates the optimal output videos.

Qualitative Results We qualitatively compare our method against the baselines in Fig. 8. Our method generate videos that match the structure and layout of the input video while faithfully adhering to the edit prompt, while other methods struggle to maintain the structural and motion integrity of the original video. As all three methods employ unaltered temporal interpolation and super-resolution models following the generation of keyframes, they commonly produce temporally consistent videos. Refer to Supplementary Material and project page for full results.

Quantitative Results Adopting the metrics outlined in Sec. 4.1, we conduct a quantitative comparison of our method against baseline approaches, detailed in Tab. 1. Notably, our approach demonstrated substantial superiority in Structure and Motion Preservation (SM-Preserve).

4.3 Ablation Studies

In Fig. 6, we evaluate the impact of using binary masks to selectively filter gradients during \mathcal{L}_{V-DDS} update. The results demonstrate that filtering gradients

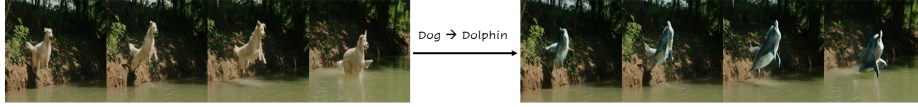


Fig. 10: Limitation. Our method limits its ability to produce videos that necessitate substantial structural alterations.

responsible for appearance injection enhances the precision of video editing and improves visual fidelity, while avoiding issues of blurriness and saturation.

We next ablate the necessity of our self-similarity guidance. Fig. 3 illustrates the optimization progress with and without our self-similarity alignments. The process begins with the initial input video (top row). Solely using \mathcal{L}_{V-DDS} for appearance injection (left) leads to the accumulation of structural errors as optimization progresses, resulting in motion deviation in the final output. However, when the process is regularized by the spatial and temporal self-similarities (right), edited videos maintain the structure and motion fidelity throughout the optimization. Additionally, in Fig. 9, we illustrate video editing results under different optimization setups: (i) \mathcal{L}_{V-DDS} . (ii) $\mathcal{L}_{V-DDS} + \mathcal{L}_{S-SSM}$. (iii) $\mathcal{L}_{V-DDS} + \mathcal{L}_{S-SSM} + \mathcal{L}_{T-SSM}$. Absence of spatial self-similarity loss leads to inconsistency in object structures across frames. For instance, the shape of a bird’s wing varies, creating visible discrepancies, as shown in Fig. 9-*left*. While aligning spatial self-similarity with the original video preserves structural integrity, it may generate artifacts in optimized areas. However, these artifacts are efficiently addressed through the addition of temporal self-similarity guidance.

5 Conclusion

In this work, we have addressed the intricate challenge of diffusion-based video editing, a domain where formulating temporally consistent, real-world motion remains a notable obstacle. DreamMotion introduced score distillation based optimization to text-to-video diffusion models, marking a departure from traditional, ancestral sampling based video editing. Our framework adeptly incorporated new content as specified by target text descriptions using Video Delta Denoising Score, while preserving the structural integrity and motion of the original video via a novel space-time self-similarity alignment. Through rigorous validation in both cascaded and non-cascaded video diffusion settings, our approach has proven superior in maintaining the essence of the original video while seamlessly integrating desired alterations. Regarding limitations, our framework is designed to preserve structural integrity of the original video, and as such, it is not suited for edits that require significant structural changes (see Fig. 10).

Ethics Statement. Our work is based on generative models that carry the risk of being repurposed for unethical uses, including the creation of misleading or counterfeit content, which may yield adverse societal impacts.

References

1. Bain, M., Nagrani, A., Varol, G., Zisserman, A.: Frozen in time: A joint video and image encoder for end-to-end retrieval. In: IEEE International Conference on Computer Vision (2021)
2. Blattmann, A., Rombach, R., Ling, H., Dockhorn, T., Kim, S.W., Fidler, S., Kreis, K.: Align your latents: High-resolution video synthesis with latent diffusion models. In: Proceedings of the IEEE/CVF Conference on Computer Vision and Pattern Recognition. pp. 22563–22575 (2023)
3. Caron, M., Touvron, H., Misra, I., Jégou, H., Mairal, J., Bojanowski, P., Joulin, A.: Emerging properties in self-supervised vision transformers. In: Proceedings of the IEEE/CVF international conference on computer vision. pp. 9650–9660 (2021)
4. Ceylan, D., Huang, C.H.P., Mitra, N.J.: Pix2video: Video editing using image diffusion. In: Proceedings of the IEEE/CVF International Conference on Computer Vision. pp. 23206–23217 (2023)
5. Chen, H., Xia, M., He, Y., Zhang, Y., Cun, X., Yang, S., Xing, J., Liu, Y., Chen, Q., Wang, X., et al.: Videocrafter1: Open diffusion models for high-quality video generation. arXiv preprint arXiv:2310.19512 (2023)
6. Chen, R., Chen, Y., Jiao, N., Jia, K.: Fantasia3d: Disentangling geometry and appearance for high-quality text-to-3d content creation. arXiv preprint arXiv:2303.13873 (2023)
7. Chen, W., Wu, J., Xie, P., Wu, H., Li, J., Xia, X., Xiao, X., Lin, L.: Control-a-video: Controllable text-to-video generation with diffusion models. arXiv preprint arXiv:2305.13840 (2023)
8. Cong, Y., Xu, M., Simon, C., Chen, S., Ren, J., Xie, Y., Perez-Rua, J.M., Rosenhahn, B., Xiang, T., He, S.: Flatten: optical flow-guided attention for consistent text-to-video editing. arXiv preprint arXiv:2310.05922 (2023)
9. Esser, P., Chiu, J., Atighehchian, P., Granskog, J., Germanidis, A.: Structure and content-guided video synthesis with diffusion models. In: Proceedings of the IEEE/CVF International Conference on Computer Vision. pp. 7346–7356 (2023)
10. Geyer, M., Bar-Tal, O., Bagon, S., Dekel, T.: Tokenflow: Consistent diffusion features for consistent video editing. arXiv preprint arXiv:2307.10373 (2023)
11. Hertz, A., Aberman, K., Cohen-Or, D.: Delta denoising score. In: Proceedings of the IEEE/CVF International Conference on Computer Vision. pp. 2328–2337 (2023)
12. Hessel, J., Holtzman, A., Forbes, M., Bras, R.L., Choi, Y.: Clipscore: A reference-free evaluation metric for image captioning. arXiv preprint arXiv:2104.08718 (2021)
13. Ho, J., Chan, W., Saharia, C., Whang, J., Gao, R., Gritsenko, A., Kingma, D.P., Poole, B., Norouzi, M., Fleet, D.J., et al.: Imagen video: High definition video generation with diffusion models. arXiv preprint arXiv:2210.02303 (2022)
14. Ho, J., Jain, A., Abbeel, P.: Denoising diffusion probabilistic models. *Advances in neural information processing systems* **33**, 6840–6851 (2020)
15. Ho, J., Salimans, T.: Classifier-free diffusion guidance. arXiv preprint arXiv:2207.12598 (2022)
16. Ho, J., Salimans, T., Gritsenko, A., Chan, W., Norouzi, M., Fleet, D.J.: Video diffusion models. arXiv:2204.03458 (2022)
17. Hu, Z., Xu, D.: Videocontrolnet: A motion-guided video-to-video translation framework by using diffusion model with controlnet. arXiv preprint arXiv:2307.14073 (2023)

18. Huang, Y., Wang, J., Shi, Y., Qi, X., Zha, Z.J., Zhang, L.: Dreamtime: An improved optimization strategy for text-to-3d content creation. arXiv preprint arXiv:2306.12422 (2023)
19. Hyvärinen, A., Dayan, P.: Estimation of non-normalized statistical models by score matching. *Journal of Machine Learning Research* **6**(4) (2005)
20. Jeong, H., Park, G.Y., Ye, J.C.: Vmc: Video motion customization using temporal attention adaption for text-to-video diffusion models. arXiv preprint arXiv:2312.00845 (2023)
21. Jeong, H., Ye, J.C.: Ground-a-video: Zero-shot grounded video editing using text-to-image diffusion models. arXiv preprint arXiv:2310.01107 (2023)
22. Khachatryan, L., Movsisyan, A., Tadevosyan, V., Henschel, R., Wang, Z., Navasardyan, S., Shi, H.: Text2video-zero: Text-to-image diffusion models are zero-shot video generators. arXiv preprint arXiv:2303.13439 (2023)
23. Kim, S., Lee, K., Choi, J.S., Jeong, J., Sohn, K., Shin, J.: Collaborative score distillation for consistent visual synthesis. arXiv preprint arXiv:2307.04787 (2023)
24. Kolkin, N., Salavon, J., Shakhnarovich, G.: Style transfer by relaxed optimal transport and self-similarity. In: *Proceedings of the IEEE/CVF Conference on Computer Vision and Pattern Recognition*. pp. 10051–10060 (2019)
25. Kwon, G., Ye, J.C.: Diffusion-based image translation using disentangled style and content representation. arXiv preprint arXiv:2209.15264 (2022)
26. Li, Y., Liu, H., Wu, Q., Mu, F., Yang, J., Gao, J., Li, C., Lee, Y.J.: Gligen: Open-set grounded text-to-image generation. In: *Proceedings of the IEEE/CVF Conference on Computer Vision and Pattern Recognition*. pp. 22511–22521 (2023)
27. Lin, C.H., Gao, J., Tang, L., Takikawa, T., Zeng, X., Huang, X., Kreis, K., Fidler, S., Liu, M.Y., Lin, T.Y.: Magic3d: High-resolution text-to-3d content creation. In: *Proceedings of the IEEE/CVF Conference on Computer Vision and Pattern Recognition*. pp. 300–309 (2023)
28. Liu, S., Zhang, Y., Li, W., Lin, Z., Jia, J.: Video-p2p: Video editing with cross-attention control. arXiv preprint arXiv:2303.04761 (2023)
29. Materzynska, J., Sivic, J., Shechtman, E., Torralba, A., Zhang, R., Russell, B.: Customizing motion in text-to-video diffusion models. arXiv preprint arXiv:2312.04966 (2023)
30. Metzger, G., Richardson, E., Patashnik, O., Giryes, R., Cohen-Or, D.: Latent-nerf for shape-guided generation of 3d shapes and textures. In: *Proceedings of the IEEE/CVF Conference on Computer Vision and Pattern Recognition*. pp. 12663–12673 (2023)
31. Mildenhall, B., Srinivasan, P.P., Tancik, M., Barron, J.T., Ramamoorthi, R., Ng, R.: Nerf: Representing scenes as neural radiance fields for view synthesis. *Communications of the ACM* **65**(1), 99–106 (2021)
32. Nam, H., Kwon, G., Park, G.Y., Ye, J.C.: Contrastive denoising score for text-guided latent diffusion image editing. arXiv preprint arXiv:2311.18608 (2023)
33. Park, J., Kwon, G., Ye, J.C.: Ed-nerf: Efficient text-guided editing of 3d scene using latent space nerf. arXiv preprint arXiv:2310.02712 (2023)
34. Podell, D., English, Z., Lacey, K., Blattmann, A., Dockhorn, T., Müller, J., Penna, J., Rombach, R.: Sdxl: Improving latent diffusion models for high-resolution image synthesis. arXiv preprint arXiv:2307.01952 (2023)
35. Pont-Tuset, J., Perazzi, F., Caelles, S., Arbeláez, P., Sorkine-Hornung, A., Van Gool, L.: The 2017 davis challenge on video object segmentation. arXiv preprint arXiv:1704.00675 (2017)
36. Poole, B., Jain, A., Barron, J.T., Mildenhall, B.: Dreamfusion: Text-to-3d using 2d diffusion. arXiv preprint arXiv:2209.14988 (2022)

37. Qi, C., Cun, X., Zhang, Y., Lei, C., Wang, X., Shan, Y., Chen, Q.: Fatezero: Fusing attentions for zero-shot text-based video editing. arXiv preprint arXiv:2303.09535 (2023)
38. Radford, A., Kim, J.W., Hallacy, C., Ramesh, A., Goh, G., Agarwal, S., Sastry, G., Askell, A., Mishkin, P., Clark, J., et al.: Learning transferable visual models from natural language supervision. In: International conference on machine learning. pp. 8748–8763. PMLR (2021)
39. Ramesh, A., Dhariwal, P., Nichol, A., Chu, C., Chen, M.: Hierarchical text-conditional image generation with clip latents. arXiv preprint arXiv:2204.06125 1(2), 3 (2022)
40. Rombach, R., Blattmann, A., Lorenz, D., Esser, P., Ommer, B.: High-resolution image synthesis with latent diffusion models. In: Proceedings of the IEEE/CVF conference on computer vision and pattern recognition. pp. 10684–10695 (2022)
41. Saharia, C., Chan, W., Saxena, S., Li, L., Whang, J., Denton, E.L., Ghasemipour, K., Gontijo Lopes, R., Karagol Ayan, B., Salimans, T., et al.: Photorealistic text-to-image diffusion models with deep language understanding. Advances in Neural Information Processing Systems **35**, 36479–36494 (2022)
42. Schuhmann, C., Beaumont, R., Vencu, R., Gordon, C., Wightman, R., Cherti, M., Coombes, T., Katta, A., Mullis, C., Wortsman, M., et al.: Laion-5b: An open large-scale dataset for training next generation image-text models. Advances in Neural Information Processing Systems **35**, 25278–25294 (2022)
43. Shechtman, E., Irani, M.: Matching local self-similarities across images and videos. In: 2007 IEEE Conference on Computer Vision and Pattern Recognition. pp. 1–8. IEEE (2007)
44. Shen, T., Gao, J., Yin, K., Liu, M.Y., Fidler, S.: Deep marching tetrahedra: a hybrid representation for high-resolution 3d shape synthesis. Advances in Neural Information Processing Systems **34**, 6087–6101 (2021)
45. Singer, U., Polyak, A., Hayes, T., Yin, X., An, J., Zhang, S., Hu, Q., Yang, H., Ashual, O., Gafni, O., et al.: Make-a-video: Text-to-video generation without text-video data. arXiv preprint arXiv:2209.14792 (2022)
46. Sohl-Dickstein, J., Weiss, E., Maheswaranathan, N., Ganguli, S.: Deep unsupervised learning using nonequilibrium thermodynamics. In: International conference on machine learning. pp. 2256–2265. PMLR (2015)
47. Song, J., Meng, C., Ermon, S.: Denoising diffusion implicit models. arXiv preprint arXiv:2010.02502 (2020)
48. Song, Y., Ermon, S.: Generative modeling by estimating gradients of the data distribution. Advances in neural information processing systems **32** (2019)
49. Song, Y., Sohl-Dickstein, J., Kingma, D.P., Kumar, A., Ermon, S., Poole, B.: Score-based generative modeling through stochastic differential equations. arXiv preprint arXiv:2011.13456 (2020)
50. Sterling, S.: Zeroscope (2023), https://huggingface.co/cerspense/zeroscope_v2_576w
51. Tang, L., Jia, M., Wang, Q., Phoo, C.P., Hariharan, B.: Emergent correspondence from image diffusion. Advances in Neural Information Processing Systems **36** (2024)
52. Tsalicoglou, C., Manhardt, F., Tonioni, A., Niemeyer, M., Tombari, F.: Textmesh: Generation of realistic 3d meshes from text prompts. arXiv preprint arXiv:2304.12439 (2023)
53. Tumanyan, N., Bar-Tal, O., Bagon, S., Dekel, T.: Splicing vit features for semantic appearance transfer. In: Proceedings of the IEEE/CVF Conference on Computer Vision and Pattern Recognition. pp. 10748–10757 (2022)

54. Vincent, P.: A connection between score matching and denoising autoencoders. *Neural computation* **23**(7), 1661–1674 (2011)
55. Wang, J., Yuan, H., Chen, D., Zhang, Y., Wang, X., Zhang, S.: Modelscope text-to-video technical report. arXiv preprint arXiv:2308.06571 (2023)
56. Wang, W., Jiang, Y., Xie, K., Liu, Z., Chen, H., Cao, Y., Wang, X., Shen, C.: Zero-shot video editing using off-the-shelf image diffusion models. arXiv preprint arXiv:2303.17599 (2023)
57. Wang, Y., Chen, X., Ma, X., Zhou, S., Huang, Z., Wang, Y., Yang, C., He, Y., Yu, J., Yang, P., et al.: Lavie: High-quality video generation with cascaded latent diffusion models. arXiv preprint arXiv:2309.15103 (2023)
58. Wang, Z., Lu, C., Wang, Y., Bao, F., Li, C., Su, H., Zhu, J.: Prolificdreamer: High-fidelity and diverse text-to-3d generation with variational score distillation. *Advances in Neural Information Processing Systems* **36** (2024)
59. Wei, Y., Zhang, S., Qing, Z., Yuan, H., Liu, Z., Liu, Y., Zhang, Y., Zhou, J., Shan, H.: Dreamvideo: Composing your dream videos with customized subject and motion. arXiv preprint arXiv:2312.04433 (2023)
60. Wu, J.Z., Ge, Y., Wang, X., Lei, S.W., Gu, Y., Shi, Y., Hsu, W., Shan, Y., Qie, X., Shou, M.Z.: Tune-a-video: One-shot tuning of image diffusion models for text-to-video generation. In: *Proceedings of the IEEE/CVF International Conference on Computer Vision*. pp. 7623–7633 (2023)
61. Wu, R., Chen, L., Yang, T., Guo, C., Li, C., Zhang, X.: Lamp: Learn a motion pattern for few-shot-based video generation. arXiv preprint arXiv:2310.10769 (2023)
62. Yatim, D., Fridman, R., Tal, O.B., Kasten, Y., Dekel, T.: Space-time diffusion features for zero-shot text-driven motion transfer. arXiv preprint arXiv:2311.17009 (2023)
63. Zhang, D.J., Wu, J.Z., Liu, J.W., Zhao, R., Ran, L., Gu, Y., Gao, D., Shou, M.Z.: Show-1: Marrying pixel and latent diffusion models for text-to-video generation. arXiv preprint arXiv:2309.15818 (2023)
64. Zhang, L., Rao, A., Agrawala, M.: Adding conditional control to text-to-image diffusion models. In: *Proceedings of the IEEE/CVF International Conference on Computer Vision*. pp. 3836–3847 (2023)
65. Zhang, Y., Wei, Y., Jiang, D., Zhang, X., Zuo, W., Tian, Q.: Controlvideo: Training-free controllable text-to-video generation. arXiv preprint arXiv:2305.13077 (2023)
66. Zhang, Y., Tang, F., Huang, N., Huang, H., Ma, C., Dong, W., Xu, C.: Motioncrafter: One-shot motion customization of diffusion models. arXiv preprint arXiv:2312.05288 (2023)
67. Zhao, M., Wang, R., Bao, F., Li, C., Zhu, J.: Controlvideo: Adding conditional control for one shot text-to-video editing. arXiv preprint arXiv:2305.17098 (2023)
68. Zhao, R., Gu, Y., Wu, J.Z., Zhang, D.J., Liu, J., Wu, W., Keppo, J., Shou, M.Z.: Motiondirector: Motion customization of text-to-video diffusion models. arXiv preprint arXiv:2310.08465 (2023)
69. Zhu, J., Zhuang, P.: Hifa: High-fidelity text-to-3d with advanced diffusion guidance. arXiv preprint arXiv:2305.18766 (2023)

A Related Work

A.1 Video Editing using Diffusion Models

Creating videos from textual descriptions necessitates ensuring realistic and temporally consistent motion, posing a unique set of challenges compared to the text-driven image generative scenarios. Before the advent of publicly accessible text-to-video diffusion models, Tune-A-Video [60] was at the forefront of one-shot based video editing. They proposed to inflate image diffusion model to pseudo video diffusion model by appending temporal modules to image diffusion model [40] and reformulating spatial self-attention into spatio-temporal self-attention, facilitating inter-frame interactions. However, the inflation often falls short in achieving consistent and complete motion, as motion preservation relies implicitly on the attention mechanism during inference. Thus, the attention projection matrices within U-Net are often fine-tuned on the input videos [28, 60, 67].

Utilizing explicit visual signals to steer the video denoising process is another common technique. Pix2Video [4], for instance, incorporates self-attention features from previously edited frames into the self-attention layer of the current frame, whereas FateZero [37] retains all intermediate attention maps obtained during the input video inversion phase and integrates them into the attention layers throughout the editing stage. Others leverage pretrained image adapter networks for structurally consistent video generation. A notable example is ControlNet [64], which has been modified to accommodate a series of explicit structural indicators such as depth and edge maps. Ground-A-Video [21] takes this a step further by adapting both ControlNet and GLIGEN [26] for video editing, utilizing spatially-continuous depth maps and spatially-discrete bounding boxes.

Despite the availability of open-source text-to-video (T2V) diffusion models [5, 50, 55, 57, 63], recent endeavors frequently adopt a self-supervised strategy of fine-tuning pretrained video generative models on an input video, to accurately capture intricate, real-world motion. More specifically, several studies attempt to disentangle appearance and motion elements of videos during the self-supervised fine-tuning. For example, [59, 66, 68] split the fine-tuning phase into two distinct pathways: one dedicated to integrating the subject’s appearance into spatial modules, and the other aimed at embedding motion dynamics of a video into temporal modules within the T2V model. Additionally, other studies [20, 29] attempt to extract and learn motion information from a single or a few reference videos. VMC [20], for instance, propose to distill the motion within a video by calculating the residual vectors between consecutive frames, and refine temporal attention layers in cascaded video diffusion models.

Distinct from aforementioned approaches, DreamMotion circumvents the conventional ancestral sampling and employs Score Distillation Sampling [36] for editing appearance elements within a video.

A.2 Visual Generation using Score Distillation Sampling

Score Distillation Sampling (SDS) [36], also known as Score Jacobian Chaining, has become the go-to method for text-to-3D generation in recent years [6, 18, 27, 30, 33, 44, 52, 58]. DreamFusion [36] first proposed to distill the generative prior of pretrained text-to-image models and optimize a parametric image synthesis model, such as NeRF [31]. Despite its success, SDS often produces images that are overly saturated, blurry, and lack detail, largely due to the use of high CFG values [58].

To address these challenges, a range of derivative methods have been proposed [11, 18, 27, 30, 32, 58]. Specifically, in the context of accurate image editing, DDS [11] incorporates additional reference branch with corresponding text to refine the noisy gradient of SDS. Hifa [69], instead, utilizes an estimated clean image rather than the predicted noise to compute denoising scores. In our work, we employ a straightforward yet effective mask condition to refine DDS-generated gradients, allowing us to inject particular appearance to the video. We further ensures the preservation of the video’s original structure and motion through the novel regularization of space-time self-similarity alignment.

B Technical Details

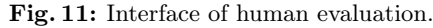
For the sampling of timestep t to derive $\mathbf{x}_t^{1:N}$ and $\hat{\mathbf{x}}_t^{1:N}$, we restrict t to the range $t \sim \mathcal{U}(0.05, 0.95)$, in line with DDS’s official implementation³. For the extraction of attention key features from video diffusion U-Net, we specifically select the self-attention layers within its decoder part. In the non-cascaded video diffusion experiments, we utilize Zeroscope⁴ [50], a diffusion model that operates in latent-space rather than pixel-space. Practically, this means the video frames are initially encoded into latent representations by VAEs, and then our proposed optimizations take place within this latent space. Conversely, in experiments involving the cascaded video diffusion framework, we select Show-1⁵ [63], where the keyframe generation UNet of Show-1 uses a pixel-space diffusion. As a result, the video frames stay in pixel space, with optimizations carried out directly within this domain.

To produce output videos using Tune-A-Video [60], ControlVideo [65], Control-A-Video [7], and TokenFlow [10], we utilized the official github repositories along with their default hyperparameters. The results from Gen-1 [9] were generated using their web-based product. Given that Gen-1 generates videos with temporally extended sequences, including duplicated frames, we removed these repeated frames when calculating CLIP-based frame consistency to ensure a fair evaluation. However, for the human evaluation, the outputs from Gen-1 were used as is, without any modifications.

³ https://github.com/google/prompt-to-prompt/blob/main/DDS_zeroshot.ipynb

⁴ https://huggingface.co/cerspense/zeroscope_v2_576w

⁵ <https://huggingface.co/showlab/show-1-base>



We carried out human evaluations to assess various methods based on three key aspects: Edit Accuracy, Frame Consistency, and Structure & Motion Preservation. Initially, we present the input video alongside its text description, as shown in Figure 11. Subsequently, we display target text with anonymized videos generated by each method and ask participants to evaluate them across the aforementioned three criteria. The human evaluation results, detailed in Table 1 of the manuscript, unequivocally highlight superiority of DreamMotion in both video diffusion frameworks.

This section is dedicated to presenting additional outcomes of DreamMotion. Figure 12 offers a comprehensive view of the results from Figure 6 in the main paper, demonstrating the effect of masking DDS-driven gradients. Annotations within the input video frames indicate the masks used. In Figure 13, we present the progress of DreamMotion optimization by visualizing intermediate output videos. Figures 14, 15, and 16 showcase input and corresponding edited videos generated with DreamMotion on Zeroscope, using various target prompts. To accommodate space constraints, only odd or even frames from 16-frame videos are selected for display. Figures 17, 18, and 19 feature videos edited by DreamMotion on the Show-1 Cascade model [63], with the left columns displaying 8-frame input videos and the adjacent columns showing 29-frame output videos. Our qualitative results are uploaded on our project page.

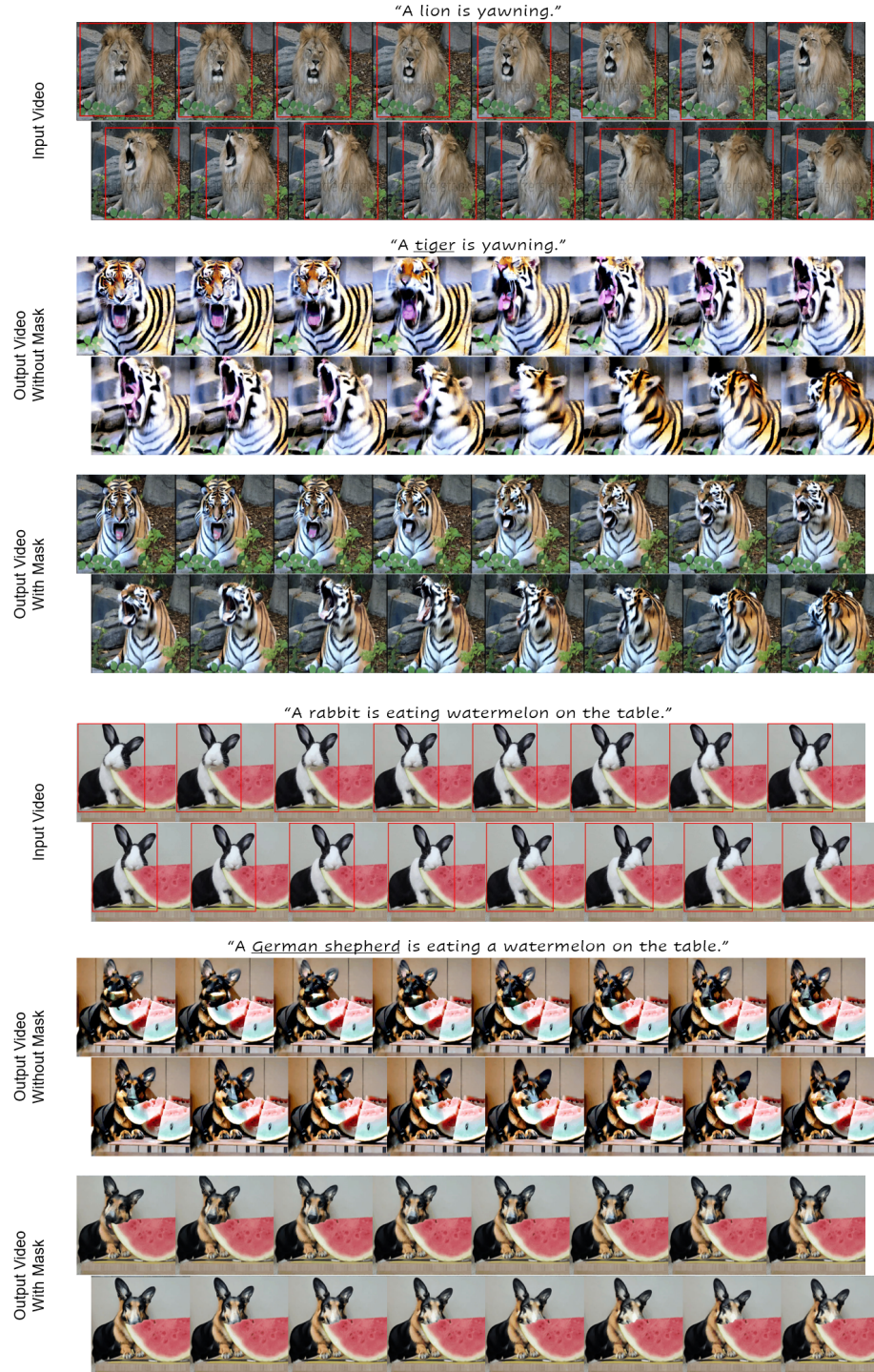


Fig. 12: Video optimization with and without masking gradients.



Fig. 13: Visualization of optimization progress.

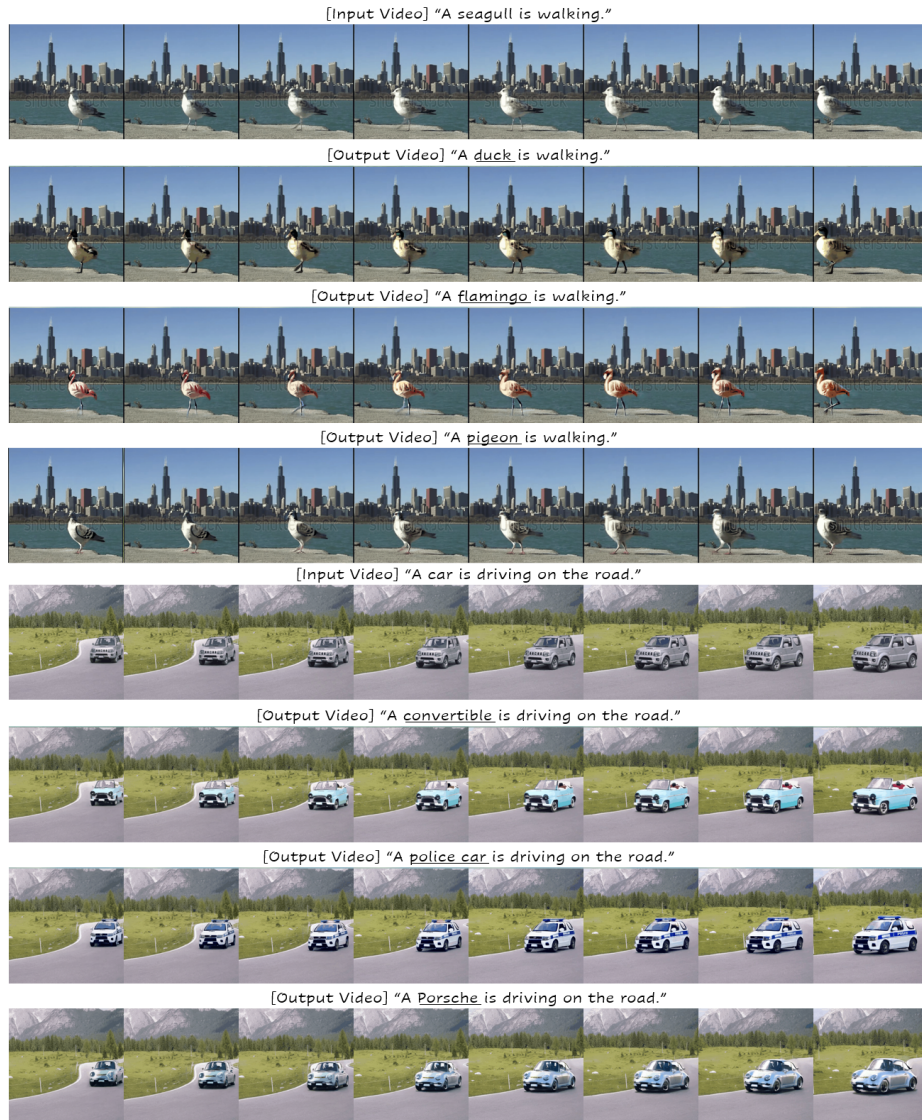


Fig. 14: Additional results of DreamMotion with Zeroscope T2V.

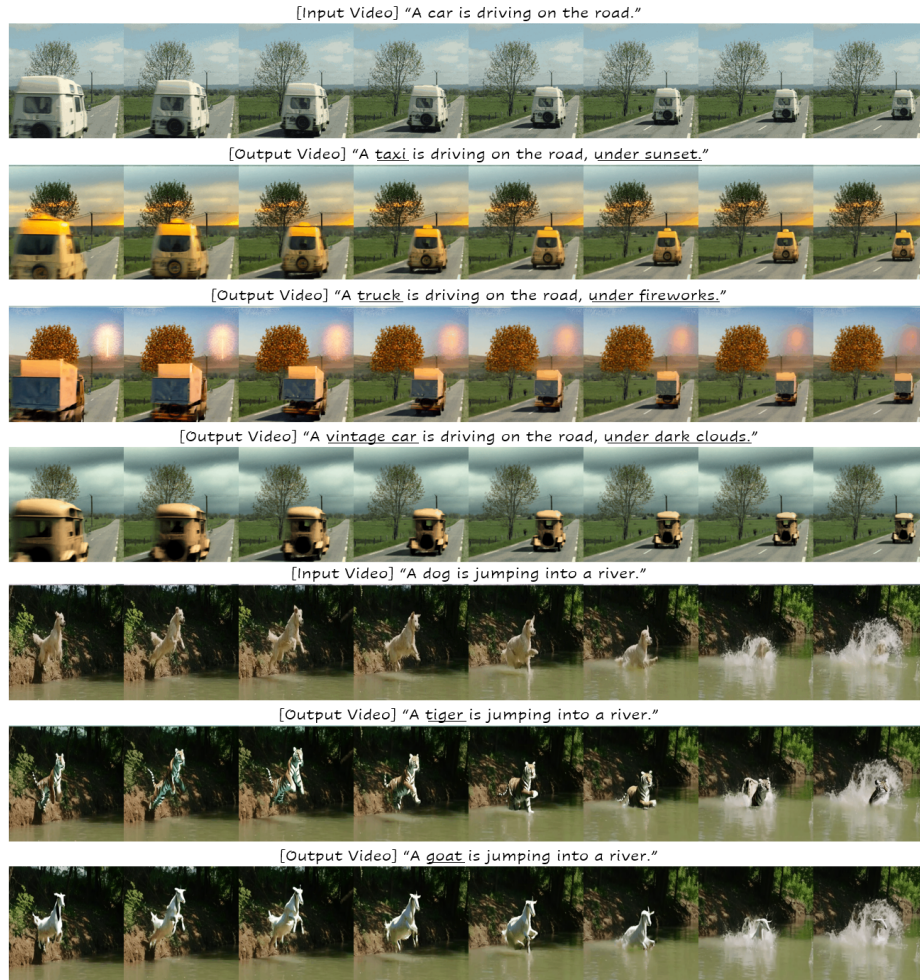


Fig. 15: Additional results of DreamMotion with Zeroscope T2V.

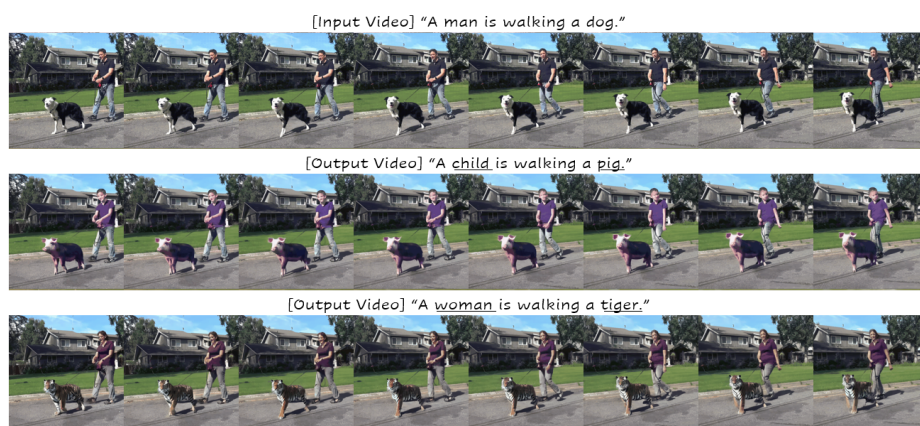


Fig. 16: Additional results of DreamMotion with Zeroscope T2V.

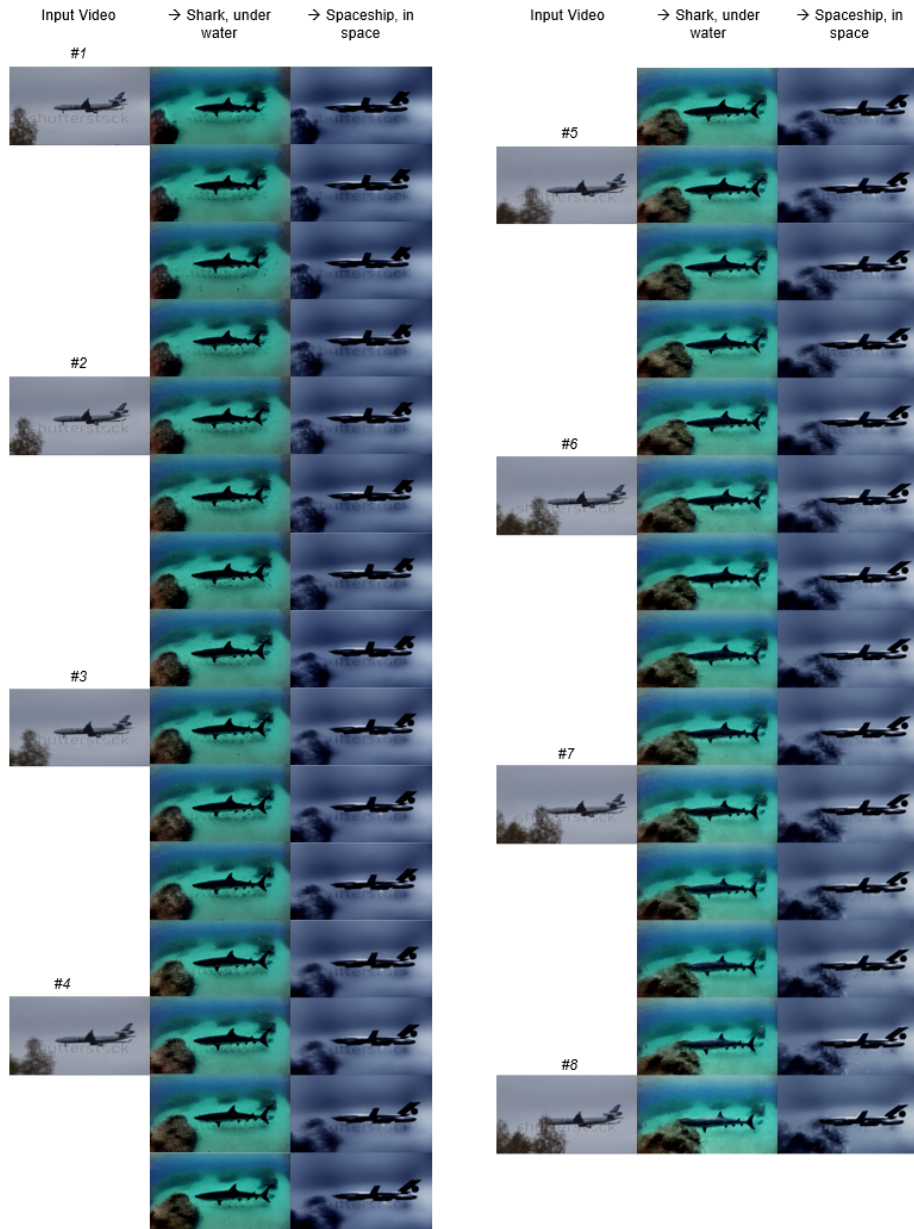


Fig. 17: Additional results of DreamMotion with Show-1 Cascade.

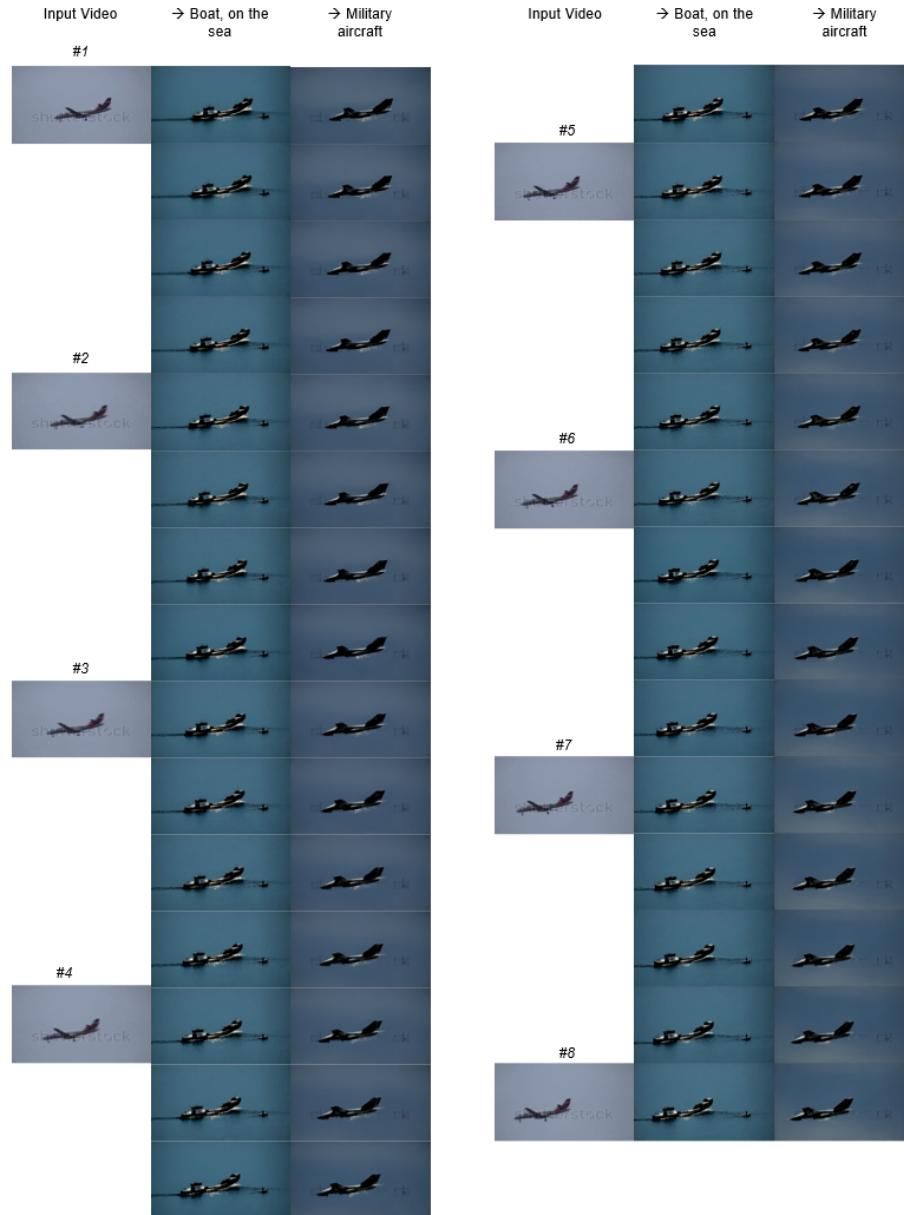


Fig. 18: Additional results of DreamMotion with Show-1 Cascade.



Fig. 19: Additional results of DreamMotion with Show-1 Cascade.